Corrosion behaviour of medium entropy alloy deposited on low carbon steel substrate by innovative welding method

4 authors:

George Simion
Universitatea Dunarea de Jos Galati
9 PUBLICATIONS **28** CITATIONS

SEE PROFILE

Julia Mirza-Rosca
Universidad de Las Palmas de Gran Canaria
71 PUBLICATIONS **439** CITATIONS

SEE PROFILE

Ionelia Voiculescu
National University of Science and Technology Politehnica Bucharest
160 PUBLICATIONS **940** CITATIONS

SEE PROFILE

Elena Scutelnicu
Universitatea Dunarea de Jos Galati
95 PUBLICATIONS **419** CITATIONS

SEE PROFILE

Corrosion behaviour of medium entropy alloy deposited on low carbon steel substrate by innovative welding method

George Simion [a], Julia Mirza-Rosca [b,c], Ionelia Voiculescu [d], Elena Scutelnicu [a,*]

[a] *Manufacturing Engineering Department, Faculty of Engineering, "Dunarea de Jos" University of Galati, 47 Domneasca St., 800008, Galati, Romania*
[b] *Mechanical Engineering Department, University of Las Palmas de Gran Canaria, 35017, Las Palmas de Gran Canaria, Spain*
[c] *Materials Engineering and Welding Department, Transilvania University of Brasov, 500036, Brasov, Romania*
[d] *Quality Engineering and Industrial Technologies Department, Faculty of Industrial Engineering and Robotics, National University of Science and Technology Politehnica of Bucharest, 060042, Bucharest, Romania*

ABSTRACT

In recent decades, thanks to the advancements within materials science and engineering, a novel class of metallic compounds, named high and medium-entropy alloys, has begun to capture the attention of researchers worldwide. Despite their excellent mechanical and anticorrosive properties, the widespread usage of these materials in industrial applications still remains a challenge and a subject worthy of investigation. In the present work, an innovative concept of developing high and medium-entropy alloys by deposition welding technique is presented and analysed in detail. Melting a bundle of rods by the Gas Tungsten Arc Welding (GTAW) method, in the same molten pool, a medium-entropy alloy (MEA) from the AlCrFeNi system is deposited on a low carbon steel substrate. In order to increase the chemical homogenization of the deposited material and to eliminate or reduce the eventual defects that may occur, electric arc remelting without using filler metal was performed in transverse, longitudinal, or combined (transverse and longitudinal) direction relative to the initial deposition welding direction. The assessment of the resistance to corrosion, modifications of microstructure, chemical composition and hardness have revealed that the medium-entropy alloy, obtained by melting in the same welding pool of several common welding rods with various chemical compositions, is an innovative, sustainable, and advantageous alternative to stainless steel materials.

1. Introduction

The increasingly severe operating conditions require more and more materials with enhanced performances, characterized by both high mechanical strength and good corrosion resistance in various environments. Therefore, it was somewhat natural to make a new step in the materials development by refining and adding small amounts of microalloying elements in the existing alloys, in order to create new classes of materials which are, generically, called High-Entropy Alloys (HEA) [1,2].

These materials have in composition a minimum of five chemical elements, each of them being within 5%–35% atomic range [3,4]. Due to the combination of diverse metallic elements in such high proportion, the configurational entropy of HEAs reaches higher values than the entropy of the traditional alloys, thereby leading to a higher tendency to form solid solutions. Moreover, the presence in the crystal lattice of

chemical elements with different atomic radii generates local stresses and distortions that can anchor or block dislocations, with the effect of strengthening the solid solution. The difference in the atomic radii of the metals that form the high entropy alloys determines a slower rate of elemental diffusion and phase transformations in comparison with the conventional alloys. Besides, a noteworthy observation is the strength of these novel materials that can be much higher than the average of the constituent metals, this effect being dependent on the elements type and their proportion. Also, the addition of five or more elements determines four main effects in terms of high entropy, severe lattice distortion, sluggish diffusion, and cocktail effects [5–7].

The special properties of HEAs, with reference to high mechanical properties [8–11], considerable toughness [12–14], wear resistance [15–18], thermal stability [19,20], corrosion resistance [21–24], and good weldability [25–29], make them promising materials for future industrial applications in various domains. In order to mitigate the

manufacturing costs associated with HEAs, a series of Medium-Entropy Alloys (MEAs) has been recently developed. This new category of materials with excellent mechanical properties usually has four or fewer primary elements which are distributed in equiatomic or near equiatomic ratios [30–33]. Besides, the grain refinement has a positive effect, enhancing the corrosion resistance of MEAs [34]. Also, the addition of trace amounts of specific chemical elements contributes to the formation of thicker passive films, thereby increasing the corrosion resistance. At the same time, applying certain heat treatments or plastic deformation a positive influence on the microstructure and texture of MEAs has been noticed [35].

The HEAs and MEAs can be achieved by different processes, such as vacuum arc remelting, powder metallurgy, induction melting, plasma sintering of powders, and additive manufacturing. The most common method for producing bulk multi-element alloys involves melting the constituent chemical elements - whether in the form of powders, bars, rods, or profiles - in electric arc furnaces under a controlled atmosphere [36]. To enhance the homogeneity of the multi-element alloys, the resulting mixture undergoes several cycles of turning and remelting [37] which increases their production costs. On the other hand, the production costs of HEAs and MEAs wires, to be used as filler metal in welding, are high due to the raw materials cost. Besides, technical issues caused by the high hardness of these alloys can occur in the rolling process. In reference [38], the researchers have reported the development of AlCoCrFeNi high-entropy alloy rod by vacuum arc remelting technique, but this method implies higher cost of fabrication, comparing to our method that uses conventional equipment and standardized rods for performing the deposition and remelting by welding. Besides, after heat treatments at 600 and 900 °C, for 4 or 6 h, the researchers [38] observed an accumulation of chemical elements at the interface with the steel substrate or a decarburization phenomenon in the Heat Affected Zone (HAZ) that can affect the corrosion resistance through the galvanic effect. Therefore, to make these alloys more affordable, the researchers have directed their studies into improving the surface quality of traditional materials, aiming to achieve HEAs and MEAs layers at much lower costs [39–41]. However, although significant progress has been made in the development and research of high and medium-entropy alloys, the technology transfer of these novel materials from laboratory to industry still remains a challenge. This may be attributed to the expensive existing manufacturing procedures that increase the cost of alloys and hinder their integration into large-scale industrial processes. Therefore, the new medium-entropy alloy, obtained by mixing several molten filler metals in the same welding pool, having various chemical compositions, turned out to be a sustainable, innovative and advantageous alternative to high-alloyed stainless steel. It is obvious that further research on the development and optimization of new manufacturing technologies, which would allow more efficient fabrication of these advanced materials is necessary.

In this paper, based on the authors' patent [42], an innovative and cost-effective procedure for developing High and Medium-Entropy Alloys (HEA and MEA) by deposition welding technique is presented and discussed in detail. Thus, melting in the same molten pool a bundle of rods by Gas Tungsten Arc Welding (GTAW) method, a multi-element alloy is deposited on low carbon steel substrate, resulting in a new material with superior properties. The present work is focused on developing an MEA from the AlCrFeNi system, the case study has been motivated by the excellent properties, high hardness, wear and corrosion resistance of this alloy group, performances that make it attractive and appropriate for industrial applications in which the steel surface with improved properties is a demand [43–45]. In industrial applications, cladding with different special alloys, such as filler metals from the Fe-Cr-Ni-Mo system, is frequently used for improving the properties of surfaces that need to be resistant to different corrosive substances or at high temperature. Based on scientific literature [46] and own previous studies [21], it was found that aluminium in addition to the alloy matrix, in certain percentages, has a beneficial role in increasing the

corrosion resistance, this information being sufficiently convincing to further investigate the microstructural and chemical changes developed in MEA from the AlCrFeNi system. Another innovative element of the research is the remelting of the weld seams, without additional filler metal, on transverse, longitudinal, or combined (transverse and longitudinal) direction relative to the initial welding direction, with the aim of chemical homogenization of the material deposited by fusion and to reduce the risk of developing potential defects. The dissimilar metals joint achieved by deposition welding of MEA layers on the low carbon steel substrate were subjected to microstructure analysis, and spectral analysis to investigate the effects of dilution and diffusion and to corrosion testing, contributing, in this way, to improvement of knowledge in the science of MEA wherein the information is almost non-existent in literature. The new medium-entropy alloy, obtained by mixing several molten filler metals in the same welding pool, having various chemical compositions, turned out to be a sustainable and innovative alternative to high-alloyed stainless steel. Based on the characterization of the MEA alloy from the AlCrFeNi system, the original and innovative results, in terms of the concept and methodology, will significantly contribute to the improvement of knowledge in the field of materials science.

2. Materials and methods

Due to its versatility, which allows the welding process in all positions, the GTAW method was selected to develop the multi-element alloy from the AlCrFeNi system, by melting the welding rods bundle with various chemical compositions onto the S235 low carbon steel substrate.

2.1. Materials

The bundle of welding rods, shown in Fig. 1, consists of three wires of 2.4 mm diameter, made of aluminum (ALTIG AL99.7), stainless-steel (INTERROD 22-9-3), and NiCr (NIROD 625) whose chemical compositions are presented in Table 1. Four plates of S235 steel with dimensions of 12x40x100, in [mm], whose chemical composition is presented in Table 2, were used as substrate for depositing the molten rods, previously mentioned. Firstly, employing a high precision balance KERN ABJ, the rods were weighed to determine the average mass which was 12.2g for the ALTIG AL99.7 aluminum rod, 35.26g for the INTERROD 22-9-3 stainless steel rod, and 36.17g for the Ni-Cr NIROD 625 alloy rod. Based on the chemical compositions, certified by the products suppliers, it was possible to make an analytic estimation of the chemical composition of the deposited metal (AlCr0.7FeNiMo0.1), as well as of the atomic ratios of the component elements, as it is shown in Table 3.

2.2. Methods

The GTAW deposition welding process was performed by employing the SAF-RO DIGIWAVE III 420 multi-process power supply. The surface of the S235 steel plates was mechanically machined in order to remove the impurities that may lead to the development of potential defects and to improve the adhesion of molten metal to the substrate. Also, to avoid the contamination of welding pool with atmospheric gases existent in the welding area, Ar shielding gas was used to create a protective atmosphere around the electric arc. As Fig. 2 illustrates, complete coverage of the substrate was obtained by partially overlapping the weld beads on approximately 50% of their width. After the GTAW welding phase was completed, the next step was to remelt, without additional filler metal, the weld beads on transverse, longitudinal, or combined (transverse and longitudinal) direction, relative to the initial welding direction (Fig. 3), aiming the chemical homogenization of the material deposited and the risk reduction of developing potential defects.

Due to the novelty of the technology that consists of simultaneous melting by GTAW of several metallic rods with different chemical compositions, in the scientific literature there is a lack of information in
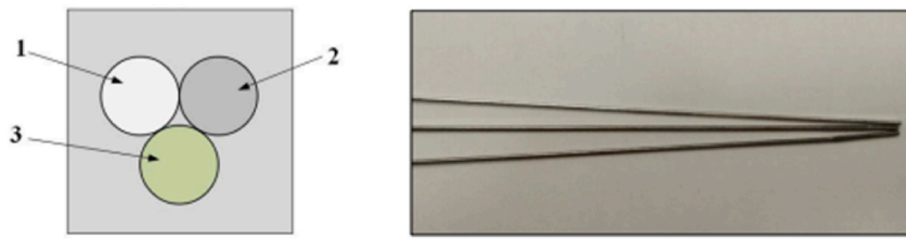
Fig. 1. Bundle of welding rods [42]: 1 – Al rod (ALTIG AL99.7); 2 – Stainless steel rod (INTERROD 22-9-3), 3 – NiCr rod (NIROD 625).

Table 1
Chemical composition of welding rods, [wt%].

Filler metal	Si	Mn	Cr	Cu	V	Ti	Al	B	Fe	Zn	Mg		
ALTIG AL99.7	0.06	0.01	0.17	0.01	0.01	0.01	99.8	0.01	0.09	0.01	0.01		
Element	Si	Mn	Cr	Cu	Ni	Mo	N	C	Fe	S	P		
INTERROD 22-9-3	0.49	1.51	23.1	0.11	8.7	3.18	0.16	0.013	62.7	0.001	0.0016		
Element	Si	Mn	Cr	Cu	Ni	Mo	Al	C	Fe	Ti	Nb	Co	S, P
NIROD 625	0.1	0.02	22.2	0.01	64.4	8.8	0.1	0.06	0.3	0.19	3.68	0.01	0.003

Table 2
Chemical composition of S235 low carbon steel.

Substrate	C	Mn	Si	P	S	Al	Cu	Cr	Ni	V	Mo	Ti	B	N	Fe
S235	0.12	0.75	0.17	0.016	0.011	0.038	0.06	0.04	0.03	0.001	0.002	0.001	0.0002	0.0064	98.22

Table 3
Chemical composition of AlCr0.7FeNiMo0.1 alloy estimated by analytic method.

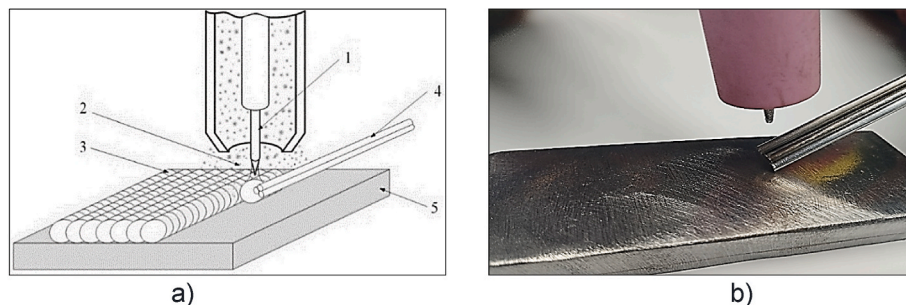| Element	C	Mn	Si	Cr	Fe	Ni	Mo	Nb	Al	N	Co	Cu	Ti
Mass, [g]	0.01	0.54	0.21	16.14	22.33	26.36	4.31	1.33	12.24	0.06	0.004	0.04	0.07
wt, [%]	0.08	0.641	0.254	19.3	26.7	31.51	5.15	1.59	14.63	0.067	0.004	0.046	0.082
at, [%]	0.03	0.58	0.45	18.37	23.37	26.18	2.66	0.85	26.84	0.24	0.004	0.04	0.08

Fig. 2. Deposition process by GTAW: a) principle of the method (1 - W electrode; 2 - shielding inert gas (Ar); 3 - layer deposited by GTAW method; 4 - bundle of metallic rods; 5 – steel substrate) [42]; b) experimental test.

terms of calculus or recommendations for the main process parameters' values. Therefore, the optimum parameters values, corresponding to the defect-free samples, have been determined by employing the DIGIWAVE III advanced welding system that allows accurate traceability and can memorize a huge number of welding programs, ensuring, in this way, a great reproducibility of welds. However, as it is well known, the welding parameters strongly depend on the grade and material thickness, as well as on the procedure and type of industrial application. Consequently, if the diameter, number or chemical composition of rods are changed, then new tests are required to set the optimal process parameters to achieve quality welded joints. After many trials, the optimum parameters that led to achieving good weld depositions were set to the following values: current intensity (I) - 220A, arc voltage (U) - 18V, welding speed (s) - 170 mm/min, and gas flow rate (Dg) - 18 l/min. Another important

parameter that has a crucial influence on the performances of welds is the inter-pass temperature which was optimised by iterative experiments, aiming to perform quality weld deposits, and further maintained at 300 °C for all samples. After each layer deposited by GTAW, the interpass-temperature was measured by employing a portable pyrometer that can ensure a maximal accuracy and process control in a large range of temperatures (50–1500 °C). Based on the data collected, the optimum process parameters determined experimentally and further applied in the deposition welding phase, followed by remelting without filler metal, are presented centralised in Table 4.

From each sample, several specimens were prepared to investigate the microstructure, chemical composition, and resistance to corrosion. The microstructure analysis was made by optical microscopy method, using the Olympus GX51 device, and by Scanning Electron Microscopy
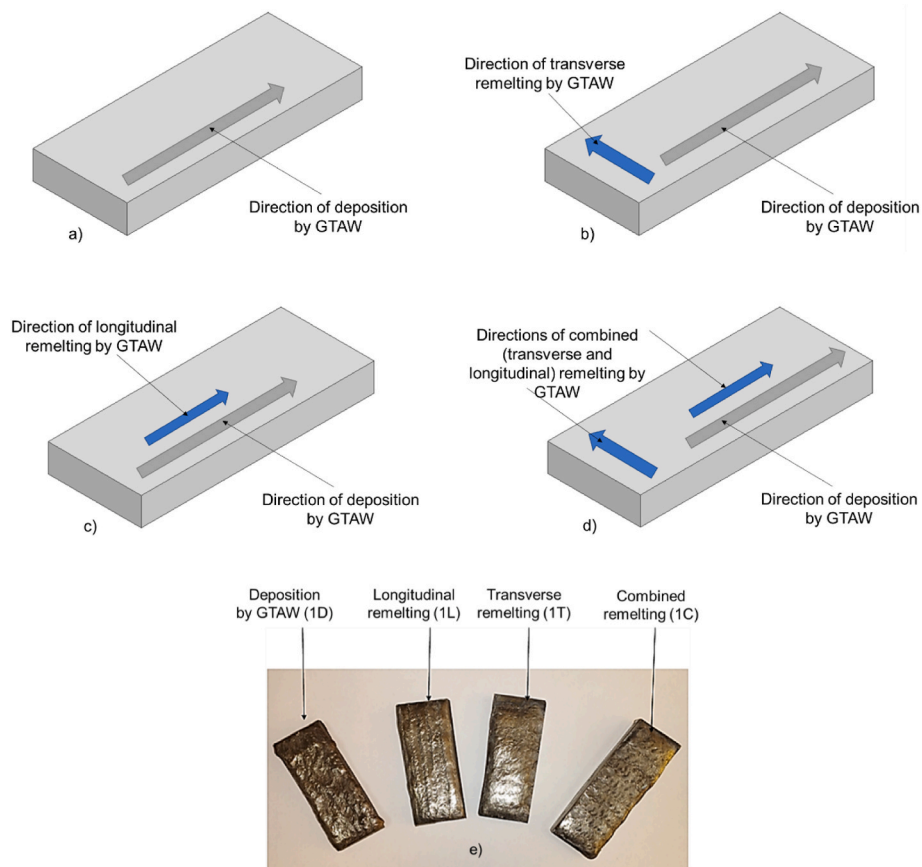
Fig. 3. Deposition welding and remelting direction: a) deposition welding without remelting; b) deposition welding followed by transverse remelting; c) deposition welding followed by longitudinal remelting; d) deposition welding followed by combined remelting; e) samples 1D, 1L, 1T, 1C.

Table 4
Process parameters applied in the deposition welding and remelting phases.

Sample code	Process		Current I [A]	Voltage U [V]	Welding speed s [cm/min]	Gas flow rate Dg [l/min]	Heat input HI [J/cm]
1D	Deposition welding		220	18	17	18	8385
1T	Transverse remelting		220	16	40	18	3168
1L	Longitudinal remelting		220	15	20	18	5940
1C (T + L)	Combined remelting:	Transverse	220	15	35	18	3394
		Longitudinal	220	18	30	18	4752

using the FEI Inspect S SEM microscope, equipped with the AMETEC Z2e chemical micro-composition EDS analyser. The sample's surfaces were sanded with Grit 400–1000 abrasive paper, followed by polishing with alpha alumina abrasive powder with granulation 1 to 0.3 μm, suspended in a water-based solution. After polishing, the specimens were cleaned with water and ethanol to eliminate the residual abrasive and lipid substances and then dried with warm air. Finally, the specimens were subjected to chemical etching with Nital 4% reagent. The microhardness testing was performed by employing the Shimadzu HMV 2T Hardness tester and applying a pressure force of 5 N and an indentation time of 10 s. Five distinct imprints of hardness were made at a minimum distance of 2.5d each other, "d" being the average value of the indentation diagonal.

The corrosion resistance of MEA achieved by GTAW deposition welding was tested in 3.5% sodium chloride (NaCl) solution, using the Biologic SP-150 potentiostat and the EC - Lab® v-9.55 software to implement the research methodology and to establish the process parameters. Additionally, this software allows the plotting of data collected, calculus of polarization resistance (*Rp*), determination of Tafel coefficients, and other electrochemical data and parameters. The tests were carried out within a special electrochemical cell equipped with three electrodes, designed for the coating specific analysis. The three electrodes consist of the coated sample to be evaluated, which plays the role of the working electrode, a saturated calomel electrode (SCE) as the reference electrode, and a platinum electrode as the counter electrode. Previously, the open circuit potential was measured by immersing the samples in the salt solution for 24 h. To confirm the findings and to ensure the research consistency, the corrosion tests were conducted three times. The linear polarization test provides information on the direct correlation between the applied polarization and the resultant current response at the corrosion potential (E_{corr}). In this study, the electrochemical measurements were conducted following the guidelines of the ASTM standard G 102-89 [47]. The potential range relative to E_{corr} was −0.25 V to 1V, with a sweep rate set of 1.66 mV/s, and the current passing through the solution of sodium chloride was continuously monitored. Furthermore, Electrochemical Impedance Spectroscopy (EIS) testing was made by measuring single sine waves at frequencies ranging from 10^{-1} to 10^5 Hz for all four samples, in conformity with the standard ISO 16773-1-4:2016 [48].

3. Results and discussion

3.1. Microstructure

Fig. 3 illustrates the fusion line characteristic of each sample, highlighting the boundary between the alloy deposited by welding and the Heat-Affected Zone (HAZ) of the substrate material. The fusion line displays a continuous profile, which is an indicator of the strong adhesion achieved between the deposited material and the substrate. Above this line, in sample 1D (Fig. 4a), it can be noticed an unmixed zone within the weld deposit, with grains that have grown from the boundary of the substrate material. The fusion line in sample 1T (Fig. 4b) appears smooth, without any visible interference or adhesion issues. A mechanical mixing of the deposited material and the substrate can be observed in the sample 1L, which was practically incorporated into the welded deposit, without mixing completely (Fig. 4c). Fig. 4d depicts the 1C sample, revealing an area wherein partial mixing of the molten alloy with the substrate metal has occurred, accompanied by the presence of small particles of intermetallic compounds within the weld deposit.

3.2. Chemical composition

The chemical analysis of samples 1D, 1T, 1L, and 1C shows notable modifications in the elemental concentrations, according to the EDS chemical analysis (cps [eV] vs. energy [keV], where cps represents the count per second), shown in Fig. 5. Specifically, an increase in the concentration of Fe from 26 wt% (the estimated Fe percentage of the alloy developed from the bundle of welding rods) to 59 wt%, accompanied by decrease in concentration of other constituents, as follows: Ni from 31 wt% to 18 wt%, Cr from 19 wt% to 12 wt%, Al from 14 wt% to 7 wt%, and Mo from 5 wt% to 2 wt% (Table 5).

These changes in chemical concentration are caused by the substrate material (structural steel S235), whose participation in the formation of the molten metal pool is approximately 45%. Besides, according to Ref. [49], the dilution of an alloy in a dissimilar metal joint is mainly influenced by the welding current intensity.

Comparable levels of dilutions have been reported in studies conducted by other researchers who deposited by the TIG welding process different alloys on dissimilar base materials [49–51]. Also, it is obvious that the remelting process will determine a higher level of dilution and a supplementary diffusion from substrate metal to the layer of MEA, demonstrated by the increase in Fe element concentration from 54% to approximately 59–61%.

Based on the SEM analysis, it was found that the main effect determined by the diffusion phenomenon between the AlCrFeNi layer and S235 steel is the enrichment with Fe of the weld deposit, the diffusion distance in the sample 1C, that was subjected to a combined remelting, being limited to approximative 10 μm, relative to the fusion line (FL). Besides, from Fig. 6a) it can be noticed that Cr, Ni, and Al chemical elements diffuse on distance of 10 μm from the MEA to the steel substrate, this phenomenon being influenced by the dilution effect, typical for the dissimilar joints performed by fusion welding procedures. Also, in the mixing zone of the MEA and the substrate material, on the distance of 10–15 μm, the grains are larger and there are no separate compounds from the metal matrix (Fig. 6a). Another noteworthy observation was the formation of Nb and Mo compounds, at the grain boundaries, only in the samples subjected to transverse and combined remelting. The formation of these compounds may be attributed to the lower heat input applied during the remelting phase of these samples.

On the other hand, in the sample 1D, carried out by welding without subsequent remelting, it was observed an accumulation of compounds enriched in Fe, in the layer deposited by GTAW, above the fusion line (Fig. 7a). The elongated conglomerate developed in the weld at 80 μm relative to the fusion line has a dilution barrier role against the diffusion of the alloying chemical elements from the MEA to the steel substrate. The chemical composition of this non-homogenous mixture (Spot 2 to Spot 4) contains Fe, as the main chemical element (80,03–84,13 wt%; 75,77–80,51 at%), Ni (4,67-7,15 wt%; 4,25-6,44 at%), Cr (4,44-5,83 wt%; 4,56-5,95 at%), Al (3,49-4,55 wt%; 6,92-8,93 at%), Si (0,84-0,91 wt%; 1,59-1,74 at%), Nb (0,44-0,49 wt%; 0,25-0,28 at%) and Mn (1,26-1,31 wt%; 1,21-1,27 at%), meaning a higher concentration of Fe and lower of other chemical elements in comparison with the percentages
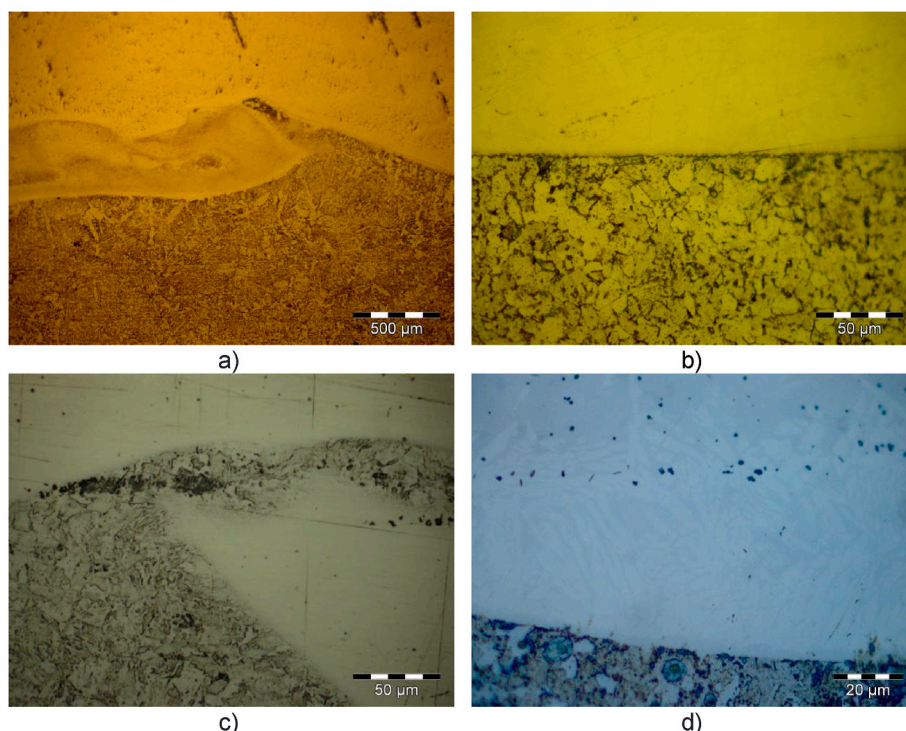

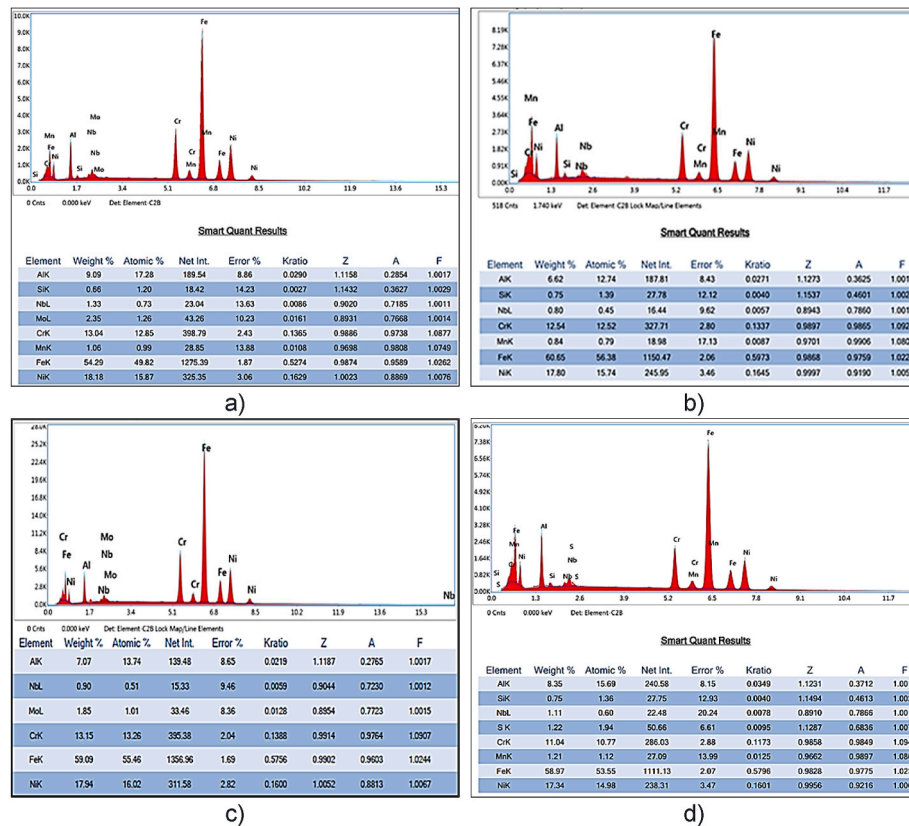**Fig. 4.** Optical image of fusion line in samples: a) 1D; b) 1T; c) 1L; d) 1C.

Fig. 5. The EDS chemical analysis in samples: a) 1D; b) 1T; c) 1L; d) 1C.

Table 5
The effect of S235 steel substrate dilution on the chemical composition of AlCr0.7FeNiMo0.1 alloy.

Material	C wt [%]	Mn wt [%]	Si wt [%]	Cr wt [%]	Fe wt [%]	Ni wt [%]	Mo wt [%]	Nb wt [%]	Al wt [%]	Co wt [%]	Cu wt [%]	Ti wt [%]
S235 substrate	0,12	0,75	0,17	0,04	98,22	0,03	0,02	–	0,038	–	0,06	0,001
$AlCr_{0,7}FeNiMo_{0,1}$ (estimated)	0,008	0,641	0,254	19,3	26,7	31,51	5,155	1,592	14,631	0,004	0,046	0,082
Sample 1D	–	–	–	13,04	54,29	18,18	2,35	1,33	9,09	–	–	–
Sample 1T	–	–	–	12,53	60,56	17,8	–	0,8	6,68	–	–	–
Sample 1L	–	–	–	13,15	59,09	17,94	1,85	0,9	7,07	–	–	–
Sample 1C	–	–	–	11,04	58,97	17,34	–	1,1	8,35	–	–	–

measured in the layers deposited by welding. This non-homogeneity phenomenon could be explained by an incomplete melting and mixture of the weld deposit. Also, from Fig. 7b), a fluctuation of Nb concentration appears within the incomplete mixing zone. The two peaks of Nb profile line may indicate the formation and segregation, in this area, of Nb-rich compounds.

On the other hand, it can be assumed that due to the participation of the structural steel substrate in weld formation, similar results would have been obtained, even if the welding rod would had been made of AlCr0.7FeNiMo0.1. Therefore, the great advantage of this innovative cladding technology, applied to achieve MEA by deposition welding, is the use of common standardized rods, instead of special rods of MEA that need longer manufacturing time and higher fabrication cost.

3.3. Hardness

The $HV_{0.5}$ microhardness testing, made on the multi-component material which consists of the structural steel S235 and the AlCr0.7Fe-NiMo0.1 medium-entropy alloy deposited by GTAW, showed an increase of 3.5 times compared to the hardness of the base material. From Fig. 8, it is observed that the average microhardness $HV_{0.5}$ exhibits a significant rise from $165HV_{0.5}$ recorded in the substrate material to $570HV_{0.5}$ in the weld deposits. The comparative analysis of hardness values revealed that the layer deposited by welding without subsequent remelting showed the lower microhardness ($558HV_{0.5}$), while the highest value, that was with 5% higher than the previous, was measured in the MEA layer that was subjected to the combined remelting. This hardening effect that makes this alloy to be adequate for industrial applications, in which the resistance to wear is a demand, can be explained by the supplementary heat introduced during the remelting process by GTAW, without filler metal. Similar hardness values of alloys AlCrFeNi, in the range 500 … 600HV, have been reported in Refs. [52,53].

3.4. Corrosion

The open circuit potential (OCP) is a method applied to achieve the corrosion potential of a material and refers to the voltage differential between the coated sample, which is considered the working electrode, and the reference electrode, in the absence of electric current. The corrosion potential of the coated sample is strongly influenced by the chemical surroundings and might modify when the coating undergoes the corrosion phenomenon. The OCP diagram, illustrating the variation
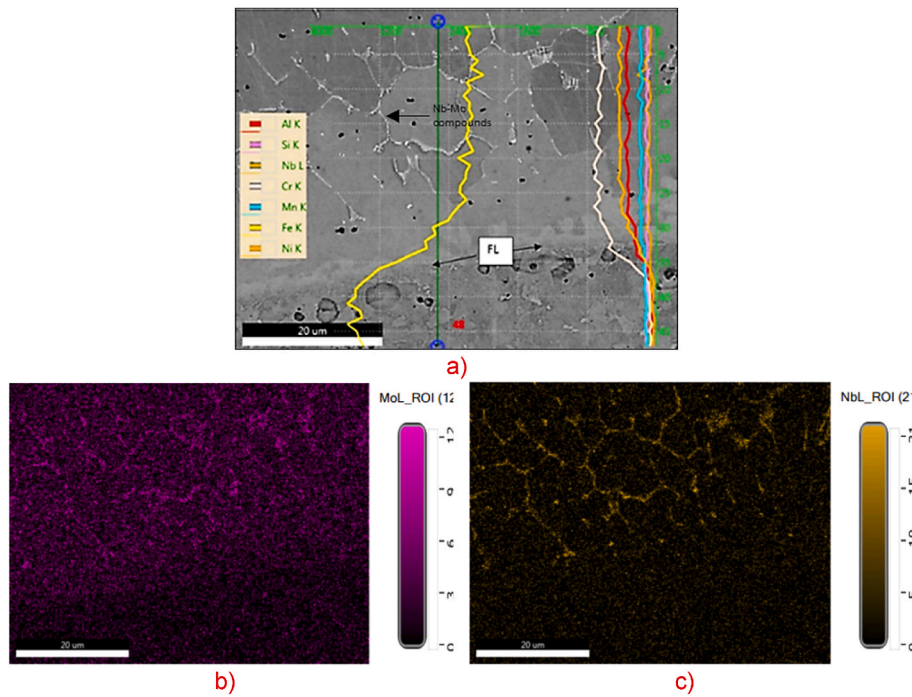
Fig. 6. Analysis of chemical composition: a) distribution of chemical elements in the transition zone from MEA to the steel substrate (sample 1C); b) and c) elemental distribution maps revealing the accumulation, in the weld deposit at the grains' boundaries, of Mo, respectively Nb chemical elements.
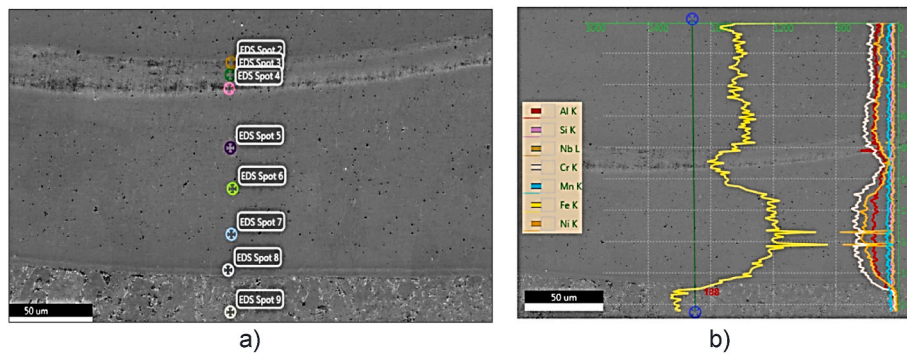

Fig. 7. Transition zone from MEA to the steel substrate (sample 1D): a) location of EDS measurement points; b) line analyse of chemical elements distribution.
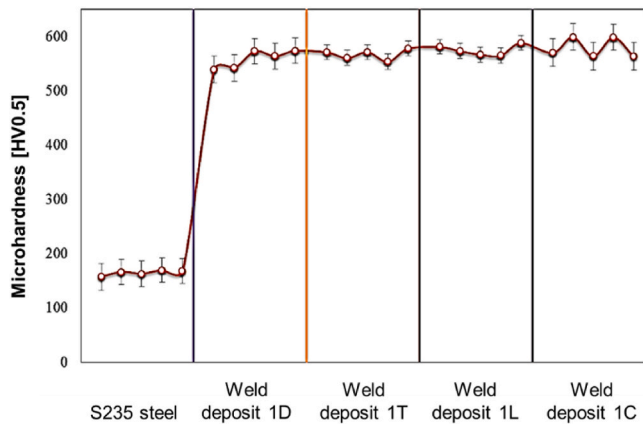

Fig. 8. Hardness profile in material substrate and MEA deposited by GTAW without remelting (1D) and with remelting (1T, 1l, 1C).

in potential as a function of time, can be built by measuring the OCP over time. Various parameters, such as the quantity of dissolved oxygen, pH level, and the presence of corrosive ions, can impact the open circuit potential of the coating in a corrosive environment.

The OCP diagrams, corresponding to the samples 1D, 1T, 1L, and 1C, are displayed in Fig. 9. As it can be seen, the potential of all samples exhibits fluctuations over time, illustrating the corrosion in the sodium chloride environment (NaCl), as well as the formation of a passive layer on the surface. After around 15 h, the OCP diagrams for the samples 1T, 1L, and 1C exhibit a rather steady potential, suggesting that the MEA alloys deposited by welding are not undergoing active corrosion and, hence, the materials show a considerable level of resistance to corrosion under these specific testing conditions. For the sample 1D, made without subsequent remelting it can be observed that the OCP graph is sharply decreasing in the last 2 h, suggesting a strong corrosion process occurred on the surface of the sample 1D.

The shape of the polarization curve can provide important information about the electrochemical behaviour of the alloy investigated. In Fig. 10 are presented the polarization curves for the coated samples. The fit of the curves is based on the Stern and Geary equation which reveals that the difference between the applied potential and the open circuit
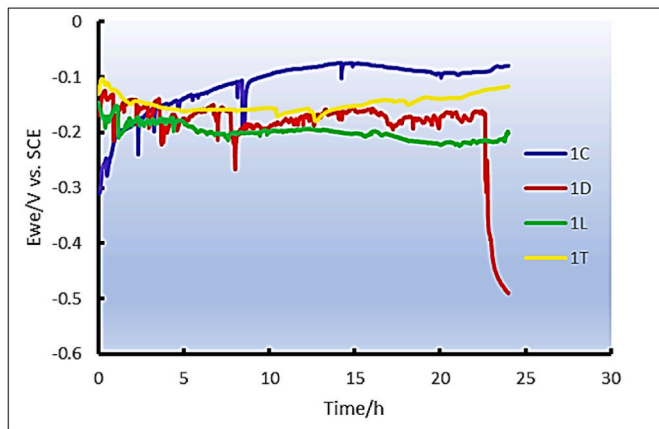
Fig. 9. OCP diagram for coated samples immersed in 3.5% NaCl solution for 24 h.
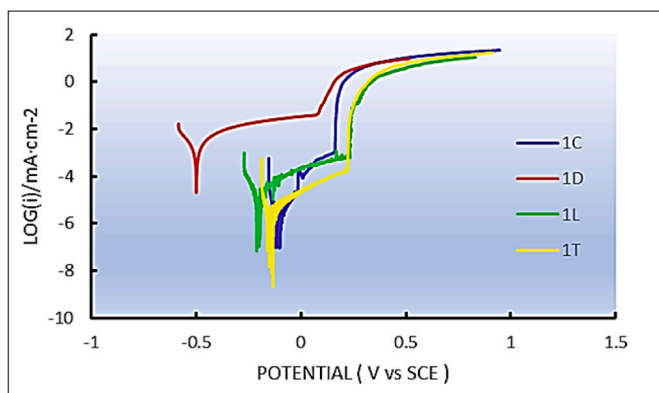

Fig. 10. Linear polarization curves of the coated samples.

potential correlates with the logarithm of the current measured during electrochemical reaction [54].

For all samples, the Tafel slopes (βa and βc) were determined by analysing the dynamic polarization curves within the range of ± 250 mV relative to the open circuit potential. The data obtained from the corrosion testing are summarized in Table 6, where: β_a and β_c represent the Tafel slopes (anodic and cathodic, respectively); E_{corr} - corrosion potential; I_{corr} - corrosion current density and V_{corr} - corrosion rate. A coated alloy exhibiting a tendency for passivation has always a higher value of β_a in comparison with βc. In scenarios where the calculated value for the slope β_a exceeds βc, and the difference is notable, as noticed for samples 1T, 1L, and 1C, it can be stated that the MEA under investigation exhibits a clear tendency towards passivation by forming a protective surface layer. This protective layer has a great role in corrosion, due to the slow down or even the prevention of the corrosive process. However, failure to simultaneously satisfy both conditions, it can suggest a susceptibility of the material to corrosion phenomenon, as it was observed in the case of sample 1D [55].

A comparative analysis of V_{corr} values, with values collected in

Table 6
Experimental data collected by corrosion testing of AlCr0.7FeNiMo0.1 alloy layers.

Sample code	βa [mV]	βc [mV]	E_{corr} [mV]	I_{corr} [$\mu A/cm^2$]	V_{corr} [mm/year]
1D	109,6	86,5	−499,764	1,096	0,0213
1L	103,6	58,2	−203,802	0,012	0,234 E−03
1T	66,1	29,4	−148,176	0,001	0,019 E−03
1C	66,2	33,7	−110,468	0,002	0,039 E−03

similar testing conditions and reported in references [56,57], demonstrates that the corrosion resistance of the coatings performed by this innovative method is even higher than of SS304, SS316L, SSMn7N-Ni, SSMn4N, SSMn6N-Ni steels. Moreover, the deposited layers exhibited superior performance compared to the bulk AlCrFeNi alloy produced via electric arc furnace that provided a corrosion current density of 0.178 $\mu A/cm^2$ during testing in a 3.5% NaCl solution [58]. This improvement can be attributed to the beneficial effects of microalloying elements contained by the welding rods used in deposition by GTAW, such as Nb and Mo that act as dissolution blockers.

The higher welding speed applied to remelt the MEA layers on transverse direction has determined, in comparison with the samples performed only by deposition welding or deposition welding followed by longitudinal remelting, an increased cooling rate and, further, a more refined grain structure. As it was reported in Ref. [59], a finer grain structure may be associated with improved corrosion resistance in certain cases. On the contrary, other researchers have suggested that a larger grain size may lead to the improvement of corrosion resistance [60,61]. However, the consensus achieved in the scientific literature shows that an optimum grain size must be obtained when the main goal of the application is to maximize the corrosion resistance. The number of studies regarding the heat input influence on MEA corrosion resistance is limited, but the research focused on stainless steels [62,63] indicates that an increase in heat input correlates with a decrease in corrosion resistance. In the present work, it was found that the lower heat input, applied in the cases of samples subjected to transverse or combined remelting, after deposition welding, is associated with higher corrosion resistance, confirming the conclusion highlighted in Refs. [62,63]. Moreover, the enhanced corrosion resistance achieved only in the samples subjected to transverse or combined remelting can also be explained by the formation, at the grain boundaries, of compounds containing the chemical elements Nb and Mo as it was presented in Fig. 6.

Another method to assess the corrosion resistance of the alloys achieved by deposition welding is the analysis of the impedance data. Upon analysing the Nyquist plots, shown in Fig. 11, it becomes obvious that all samples have two clearly distinguishable zones. The first zone refers to the area characterized by low impedances at high frequencies, whereas the second zone shows the area where the impedance has medium and high values. This pattern unambiguously suggests that there is at least one frequency-dependent activity that is contributing to the feedback. Thus, the Nyquist curves allow an analysis of the polarization resistance, which is closely related to the rate of electrochemical
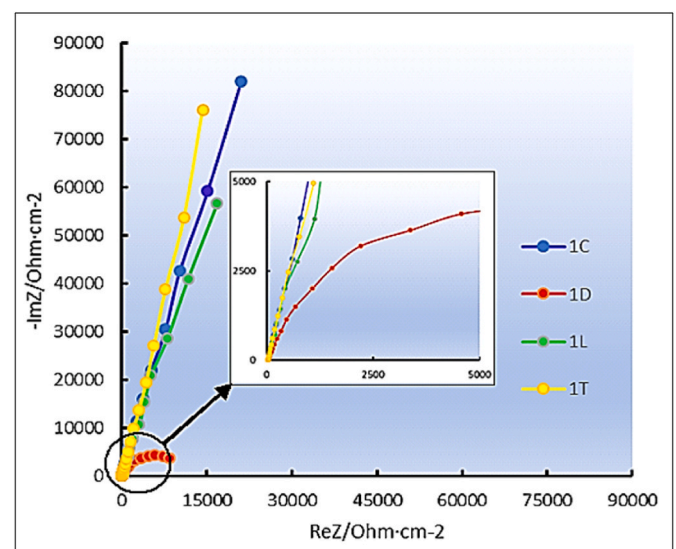

Fig. 11. Nyquist curves for the coated samples.

reactions at the metal-electrolyte interface. A high polarization resistance indicates a slowed electrochemical reaction, which can be interpreted as an indicator of good corrosion resistance. Ideally, a material with perfect corrosion resistance would be graphed by a 90-degree slope. The Nyquist curves from Fig. 11 illustrate that samples 1T, 1L, and 1C have the best corrosion resistance, while sample 1D shows a clear deterioration and a possible penetration of the coating. These results confirm clearly the data provided and discussed in the previous paragraphs.

In the Bode-IZI chart, shown in Fig. 12, the impedance spectra for all samples display overlapping curves at high frequencies, representing the electrolyte resistance, which is the same for all samples. The impedance within the low-frequency range is determined by the inherent properties of the passive film as shown in the Bode-IZI chart. The low-frequency zone represents the combined resistance of the passive film and electrolyte. Assuming that the final resistance remains consistent across all samples, any change observed in the low-frequency range can be attributed to modifications in the passive layer. These modifications may be caused by the presence of conductive channels inside the passive film. The low-frequency impedance for sample 1D decreased by about 10 times, indicating a reduced corrosion resistance of the coating. On the contrary, the samples with transversal, longitudinal, and combined subsequent remelting exhibit the highest corrosion resistance, confirming the conclusions drawn previously.

In the Bode-phase diagrams (Fig. 13), the typical behaviour of the initial nucleation of a passive layer on the surface of the metal is observed at the corrosion potential. For the remelted samples (1T, 1L, and 1C), the formed film increases in thickness and has a capacitive response illustrated by a phase angle close to 90° over a wide range of frequencies. This phenomenon is associated with an increase in the capacity, which is related to an increase in effective surface area in comparison with the sample without remelting.

4. Potential industrial applications

The remarkable properties of the Medium-Entropy Alloys (MEA), achieved by an innovative deposition welding technology, could make these materials a sustainable and advantageous alternative for many industrial applications, including repair and reconditioning of worn parts, such as.

- Machine building industry: components of production equipment (moulds, dies);
- Chemical industry: equipment for chemical processing (tanks, containers, parts for handling chemical substances);
- Energy producing industry: turbine blades;
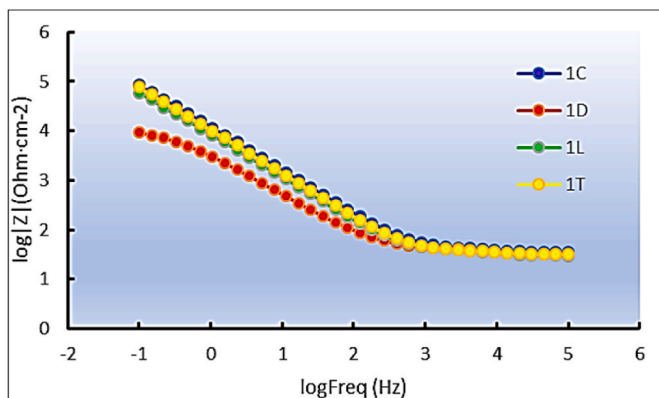- Oil and gas industry: valves, pumps, and drilling tools;
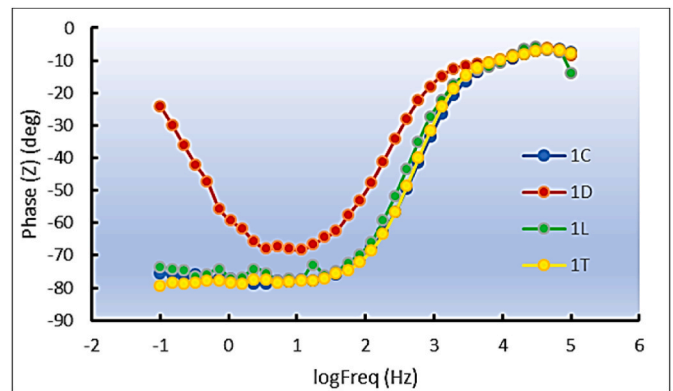

Fig. 12. Bode-IZI plots for coated samples.

Fig. 13. Bode-phase plots for coated samples.

- Ship industry: naval propellers, offshore structures, parts in contact with the marine environment;
- Mining industry: components of mining machinery and equipment.
- Industry of cellulose and paper: components for manufacturing systems, lamellae, rollers.

5. Conclusions

Based on the original and innovative scientific results discussed in this work, significant conclusions that demonstrate the high originality of the research are presented, as follows.

- By applying the innovative deposition welding technology, layers, and coatings of Medium-Entropy Alloys (MEA), with remarkable features, can be achieved and used in a wide range of industrial applications;
- Subsequent remelting of alloys deposited on the common steel substrate, by welding without filler metal, in the transverse, longitudinal, or combined (transverse and longitudinal) direction relative to the initial deposition direction with the aim of chemical homogenization and removal of potential welding defects;
- Development of a special filler metal bundle that consists of several welding rods with different chemical compositions and diameters, melted together, in the same welding pool, to achieve multi-element alloys (HEA or MEA);

The microstructure and spectral analysis, as well as the hardness and corrosion testing, applied to investigate the features of the MEA obtained by GTAW technique, have led to the following important conclusions.

- The fusion line, detected by microstructure analysis, has exhibited a continuous profile, demonstrating the strong adhesion achieved between the deposited alloy and the steel substrate. Small unmixed zones or partial mixing of the molten alloy with the substrate metal have been observed, but no any adhesion issue that may compromise the joint was identified.
- The chemical composition of the deposited alloy is highly influenced by the participation of the material substrate in the formation of the welding pool, being estimated, in this work, at approximately 45%, a usual value reported in the scientific literature for welding procedures with tungsten electrode and Ar shielding gas. Besides, the welding current is a key factor in determining the penetration (depth of fusion), increasing or decreasing, depending on the value of the amperage, the participation of the base material in forming the welded joint.
- The spectral analysis has revealed an increase of Fe percentage from 54% to 59%, after the subsequent GTAW remelting process,

confirming the influence of the remelting technology on the final chemical composition of the layer of MEA.

- The hardness testing revealed a significant increase of microhardness $HV_{0.5}$, from $165HV_{0.5}$, recorded in the substrate material, to $570HV_{0.5}$ in the weld deposits, meaning an increase of 3.5 times. Also, a hardness increase of 5% was found in the sample 1C compared to the sample 1D. This hardening effect can be explained by the supplementary heat introduced during the subsequent remelting made by GTAW that determined a modification of the grain size.

- To assess the resistance to corrosion of the MEA, deposited by welding, all samples were immersed in a solution of 3.5% NaCl for 24 h. Based on the information achieved by analysis of the open circuit potential diagram for the coated samples, linear polarization curves, Nyquist curves, Bode-IZI plots, and Bode-phase plots, it can be concluded that the multi-element alloy AlCr0.7FeNiMo0.1, deposited and remelted by welding, is characterised by a good resistance to corrosion, comparable or even higher than of stainless steel.

In the context of a sustainable and economic approach, the welds depositions of AlCr0.7FeNiMo0.1 medium-entropy alloys, achieved by this innovative technology, represent a promising option for industrial applications that require materials resistant to corrosion.

Further research will be focused on the assessment of the resistance to wear of this type of alloy and it will be extended also to studying other combinations of welding rods with different chemical compositions and diameters.

Declaration of competing interest

The authors declare the following financial interests/personal relationships which may be considered as potential competing interests: Elena Scutelnicu has patent #RO135988 issued to Dunarea de Jos University of Galati, Romania. If there are other authors, they declare that they have no known competing financial interests or personal relationships that could have appeared to influence the work reported in this paper.

References

[1] Yeh J-W, Chen S-K, Lin S-J, Gan J-Y, Chin T-S, Shun T-T, Tsau C-H, Chang S-Y. Nanostructured high-entropy alloys with multiple principal elements: novel alloy design concepts and outcomes. Adv Eng Mater 2004;6:299–303. https://doi.org/10.1002/adem.200300567.

[2] Cantor B, Chang ITH, Knight P, Vincent AJB. Microstructural development in equiatomic multicomponent alloys. Mater Sci Eng, A 2004;375–377:213–8. https://doi.org/10.1016/j.msea.2003.10.257.

[3] George EP, Raabe D, Ritchie RO. High-entropy alloys. Nat Rev Mater 2019;4: 515–34. https://doi.org/10.1038/s41578-019-0121-4.

[4] Miracle DB. High entropy alloys as a bold step forward in alloy development. Nat Commun 2019;10:1805. https://doi.org/10.1038/s41467-019-09700-1.

[5] Ye YF, Wang Q, Lu J, Liu CT, Yang Y. High-entropy alloy: challenges and prospects. Mater Today 2016;19:349–62. https://doi.org/10.1016/j.mattod.2015.11.026.

[6] Miracle DB, Senkov ON. A critical review of high entropy alloys and related concepts. Acta Mater 2017;122:448–511. https://doi.org/10.1016/j.actamat.2016.08.081.

[7] Tokarewicz M, Grądzka-Dahlke M. Review of recent research on AlCoCrFeNi high-entropy alloy. Metals 2021;11:1302. https://doi.org/10.3390/met11081302.

[8] George EP, Curtin WA, Tasan CC. High entropy alloys: a focused review of mechanical properties and deformation mechanisms. Acta Mater 2020;188: 435–74. https://doi.org/10.1016/j.actamat.2019.12.015.

[9] Li W, Xie D, Li D, Zhang Y, Gao Y, Liaw PK. Mechanical behavior of high-entropy alloys. Prog Mater Sci 2021;118:100777. https://doi.org/10.1016/j.pmatsci.2021.100777.

[10] Constantin G, Balan E, Voiculescu I, Geanta V, Craciun V. Cutting behavior of Al0.6CoCrFeNi high entropy alloy. Materials 2020;13:4181. https://doi.org/10.3390/ma13184181.

[11] Schuh B, Mendez-Martin F, Völker B, George EP, Clemens H, Pippan R, Hohenwarter A. Mechanical properties, microstructure and thermal stability of a nanocrystalline CoCrFeMnNi high-entropy alloy after severe plastic deformation. Acta Mater 2015;96:258–68. https://doi.org/10.1016/j.actamat.2015.06.025.

[12] Geantă V, Cherecheș T, Lixandru P, Voiculescu I, Ştefănoiu R, Dragnea D, Zecheru T, Matache L. Virtual testing of composite structures made of high entropy alloys and steel. Metals 2017;7:496. https://doi.org/10.3390/met7110496.

[13] Wang J, Zou J, Yang H, Dong X, Cao P, Liao X, Liu Z, Ji S. Ultrastrong and ductile (CoCrNi)94Ti3Al3 medium-entropy alloys via introducing multi-scale heterogeneous structures. J Mater Sci Technol 2023;135:241–9. https://doi.org/10.1016/j.jmst.2022.06.048.

[14] Voiculescu I, Geanta V, Chereches T, Vizureanu P, Stefanoiu R, Rotariu A, Mitrica D. Impact behavior of the ballistic targets package composed of dyneema polymer and high entropy alloy structures. Arch Metall Mater 2021:569–76. https://doi.org/10.24425/amm.2022.137792.

[15] Cheng Z, Wang S, Wu G, Gao J, Yang X, Wu H. Tribological properties of high-entropy alloys: a review. Int J Miner Metall Mater 2022;29:389–403. https://doi.org/10.1007/s12613-021-2373-4.

[16] Ayyagari A, Barthelemy C, Gwalani B, Banerjee R, Scharf TW, Mukherjee S. Reciprocating sliding wear behavior of high entropy alloys in dry and marine environments. Mater Chem Phys 2018;210:162–9. https://doi.org/10.1016/j.matchemphys.2017.07.031.

[17] Kasar AK, Scalaro K, Menezes PL. Tribological properties of high-entropy alloys under dry conditions for a wide temperature range—a review. Materials 2021;14: 5814. https://doi.org/10.3390/ma14195814.

[18] Menghani J, Vyas A, Patel P, Natu H, More S. Wear, erosion and corrosion behavior of laser cladded high entropy alloy coatings – a review. Mater Today Proc 2021;38: 2824–9. https://doi.org/10.1016/j.matpr.2020.08.763.

[19] Wolff-Goodrich S, Haas S, Glatzel U, Liebscher CH. Towards superior high temperature properties in low density ferritic AlCrFeNiTi compositionally complex alloys. Acta Mater 2021;216:117113. https://doi.org/10.1016/j.actamat.2021.117113.

[20] Mousavi SE, He AQ, Palimi M, Chen DL, Li DY. Influences of alloying elements on microstructure and tribological properties of a medium-weight high-entropy alloy. Wear 2023;524–525:204856. https://doi.org/10.1016/j.wear.2023.204856.

[21] Geantă V, Voiculescu I, Cotrut MC, Vrânceanu MD, Vasile IM, Mirza Rosca JC. Effect of Al on corrosion behavior in 3.5%NaCl solution of Al$_x$CoCrFeNi high entropy alloys. JERA 2021;53:20–30. https://dx.doi.org/10.4028/www.scientific.net/JERA.53.20.

[22] López Ríos M, Socorro Perdomo PP, Voiculescu I, Geanta V, Crăciun V, Boerasu I, Mirza Rosca JC. Effects of nickel content on the microstructure, microhardness and corrosion behavior of high-entropy AlCoCrFeNi$_x$ alloys. Sci Rep 2020;10:21119. https://doi.org/10.1038/s41598-020-78108-5.

[23] Socorro-Perdomo PP, Florido-Suárez NR, Voiculescu I, Mirza-Rosca JC. Comparative EIS study of AlxCoCrFeNi alloys in ringer's solution for medical instruments. Metals 2021;11:928. https://doi.org/10.3390/met11060928.

[24] Luo H, Li Z, Mingers AM, Raabe D. Corrosion behavior of an equiatomic CoCrFeMnNi high-entropy alloy compared with 304 stainless steel in sulfuric acid solution. Corrosion Sci 2018;134:131–9. https://doi.org/10.1016/j.corsci.2018.02.031.

[25] Guo J, Tang C, Rothwell G, Li L, Wang Y-C, Yang Q, Ren X. Welding of high entropy alloys—a review. Entropy 2019;21:431. https://doi.org/10.3390/e21040431.

[26] Scutelnicu E, Simion G, Rusu CC, Gheonea MC, Voiculescu I, Geanta V. High entropy alloys behaviour during welding. Rev. Chim. 2001;71:219–33. https://doi.org/10.37358/RC.20.3.7991.

[27] Li J, Meng X, Wan L, Huang Y. Welding of high entropy alloys: progresses, challenges and perspectives. J Manuf Process 2021;68:293–331. https://doi.org/10.1016/j.jmapro.2021.05.042.

[28] Rhode M, Richter T, Schroepfer D, Manzoni AM, Schneider M, Laplanche G. Welding of high-entropy alloys and compositionally complex alloys—an overview. Weld World 2021;65:1645–59. https://doi.org/10.1007/s40194-021-01110-6.

[29] Voiculescu I, Geanta V, Stefanescu EV, Simion G, Scutelnicu E. Effect of diffusion on dissimilar welded joint between Al0.8CoCrFeNi high-entropy alloy and S235JR structural steel. Metals 2022;12:548. https://doi.org/10.3390/met12040548.

[30] Garcia Filho FDC, Ritchie RO, Meyers MA, Monteiro SN. Cantor-derived medium-entropy alloys: bridging the gap between traditional metallic and high-entropy alloys. J Mater Res Technol 2022;17:1868–95. https://doi.org/10.1016/j.jmrt.2022.01.118.

[31] Bracq G, Laurent-Brocq M, Varvenne C, Perrière L, Curtin WA, Joubert J-M, Guillot I. Combining experiments and modeling to explore the solid solution strengthening of high and medium entropy alloys. Acta Mater 2019;177:266–79. https://doi.org/10.1016/j.actamat.2019.06.050.

[32] Ondicho I, Alunda B, Park N. Effect of Fe on the Hall-petch relationship of (CoCrMnNi) Fe medium-and high-entropy alloys. Intermetallics 2021;136:107239. https://doi.org/10.1016/j.intermet.2021.107239.

[33] Bae JW, Kim HS. Towards ferrous medium-entropy alloys with low-cost and high-performance. Scripta Mater 2020;186:169–73. https://doi.org/10.1016/j.scriptamat.2020.05.030.

[34] Wu M, Setiawan RC, Li DY. Benefits of passive element Ti to the resistance of AlCrFeCoNi high-entropy alloy to corrosion and corrosive wear. Wear 2022; 492–493:204231. https://doi.org/10.1016/j.wear.2021.204231.

[35] Saha J, Saha R, Malladi SRK, Bhattacharjee PP. Microstructure and texture of CoCrNi medium entropy alloy (MEA) processed by severe cryo-rolling: a study vis-a-vis cold-rolling. Intermetallics 2021;138:107345. https://doi.org/10.1016/j.intermet.2021.107345.

[36] Hou L, Hui J, Yao Y, Chen J, Liu J. Effects of boron content on microstructure and mechanical properties of AlFeCoNiBx high entropy alloy prepared by vacuum arc melting. Vacuum 2019;164:212–8. https://doi.org/10.1016/j.vacuum.2019.03.019.

[37] Güler S, Alkan ED, Alkan M. Vacuum Arc melted and heat treated AlCoCrFeNiTiX based high-entropy alloys: thermodynamic and microstructural investigations. J Alloys Compd 2022;903:163901. https://doi.org/10.1016/j.jallcom.2022.163901.

[38] Voiculescu I, Geanta V, Vasile IM, Stefanoiu R, Tonoiu M. Characterisation of weld deposits using as filler metal a high entropy alloy. J Optoelectron Adv Mater 2013; 15:650–4.

[39] Arif ZU, Khalid MY, Ur Rehman E, Ullah S, Atif M, Tariq A. A review on laser cladding of high-entropy alloys, their recent trends and potential applications. J Manuf Process 2021;68:225–73. https://doi.org/10.1016/j.jmapro.2021.06.041.

[40] Wen X, Cui X, Jin G, Zhang X, Zhang Y, Zhang D, Fang Y. Design and characterization of FeCrCoAlMn0.5Mo0.1 high-entropy alloy coating by ultrasonic assisted laser cladding. J Alloys Compd 2020;835:155449. https://doi.org/10.1016/j.jallcom.2020.155449.

[41] Liu J, Liu H, Chen P, Hao J. Microstructural characterization and corrosion behaviour of AlCoCrFeNiTix high-entropy alloy coatings fabricated by laser cladding. Surf Coating Technol 2019;361:63–74. https://doi.org/10.1016/j.surfcoat.2019.01.044.

[42] Scutelnicu E, Simion G, Mircea O, Rusu CC, Mistodie LR, Gheonea MC, Geanta V, Voiculescu I. Procedeu de Realizare a Unei Depuneri Din Aliaj Multielement Tip AlCrFeNi Prin Topire Cu Arc Electric in Mediu de Gaz Protector Inert (Procedure for Obtaining Deposition of AlCrFeNi Multi-Element Alloy by Fusion with Electric Arc and Inert Shielding Gas). 2024.

[43] Dong Y, Lu Y, Kong J, Zhang J, Li T. Microstructure and mechanical properties of multi-component AlCrFeNiMox high-entropy alloys. J Alloys Compd 2013;573: 96–101. https://doi.org/10.1016/j.jallcom.2013.03.253.

[44] Yuan J, Yang Y, Duan S, Dong Y, Li C, Zhang Z. Rapid design, microstructures, and properties of low-cost Co-free Al-Cr-Fe-Ni eutectic medium entropy alloys. Materials 2022;16:56. https://doi.org/10.3390/ma16010056.

[45] Tang Y, Wang S, Sun B, Wang Y, Qiao Y. FABRICATION AND WEAR BEHAVIOR ANALYSIS ON AlCrFeNi HIGH ENTROPY ALLOY COATING UNDER DRY SLIDING AND OIL LUBRICATION TEST CONDITIONS. Surf Rev Lett 2016;23:1650018. https://doi.org/10.1142/S0218625X16500189.

[46] Zhao J, Wu W, Cai J, Cheng X. Evaluating the effect of aluminum on the corrosion resistance of the structural steels used for marine engineering. J Mater Res Technol 2022;18:4181–93. https://doi.org/10.1016/j.jmrt.2022.04.061.

[47] Standard practice for calculation of corrosion rates and related information from electrochemical measurementsG1vols. 02–89. West Conshohocken, PA, USA: ASTM; 1999.

[48] Electrochemical impedance spectroscopy (EIS) on coated and uncoated metallic specimens. In: ISO 16773-1-4:2016; Geneva, Switzerland; 2016.

[49] Silwal B, Walker J, West D. Hot-wire GTAW cladding: inconel 625 on 347 stainless steel. Int J Adv Manuf Technol 2019;102:3839–48. https://doi.org/10.1007/s00170-019-03448-0.

[50] Xu G, Kutsuna M, Liu Z, Yamada K. Comparison between diode laser and TIG cladding of Co-based alloys on the SUS403 stainless steel. Surf Coating Technol 2006;201:1138–44. https://doi.org/10.1016/j.surfcoat.2006.01.040.

[51] Huo W, Shi H, Ren X, Zhang J. Microstructure and wear behavior of CoCrFeMnNbNi high-entropy alloy coating by TIG cladding. Adv Mater Sci Eng 2015:1–5. https://doi.org/10.1155/2015/647351.

[52] Shang CY, Wang Y. AlCrFeNi high-entropy coating fabricated by mechanical alloying and hot pressing sintering. MSF 2017;898:628–37. https://dx.doi.org/10.4028/www.scientific.net/MSF.898.628.

[53] Jumaev E, Abbas MA, Mun SC, Song G, Hong S-J, Kim KB. Nano-scale structural evolution of quaternary AlCrFeNi based high entropy alloys by the addition of specific minor elements and its effect on mechanical characteristics. J Alloys Compd 2021;868:159217. https://doi.org/10.1016/j.jallcom.2021.159217.

[54] Stern M, Geaby AL. Electrochemical polarization. J Electrochem Soc 1957;104:56. https://doi.org/10.1149/1.2428496.

[55] Jones DA. Principles and prevention of corrosion; 2. Int. Ed. Harlow: Pearson Education; 2014.

[56] Nadliriyah N, Putri AL, Triwikantoro T. PANi/ZrO$_2$-composite coating for corrosion protection in 3.5 M NaCl solution. IOP Conf Ser Mater Sci Eng 2019;496: 012059. https://doi.org/10.1088/1757-899X/496/1/012059.

[57] Saeed A. Low activation-modified high manganese-nitrogen austenitic stainless steel for fast reactor pressure vessel cladding. Nuclear Science 2018;3:45. https://doi.org/10.11648/j.ns.20180303.14.

[58] Wu M, Diao G, Yuan JF, Fraser D, Li J, Chung R, Li DY. Corrosion and corrosive wear of AlCrFeCoNi and Co-free AlCrFeNi-tix (x = 0–1.5) high-entropy alloys in 3.5 Wt % NaCl and H2SO4 (pH = 3) solutions. Wear 2023;523:204765. https://doi.org/10.1016/j.wear.2023.204765.

[59] Xue L, Ding Y, Pradeep KG, Case R, Castaneda H, Paredes M. The grain size effect on corrosion property of Al 2 Cr 5 Cu 5 Fe 53 Ni 35 high-entropy alloy in marine environment. Corrosion Sci 2022;208:110625. https://doi.org/10.1016/j.corsci.2022.110625.

[60] Parakh A, Vaidya M, Kumar N, Chetty R, Murty BS. Effect of crystal structure and grain size on corrosion properties of AlCoCrFeNi high entropy alloy. J Alloys Compd 2021;863:158056. https://doi.org/10.1016/j.jallcom.2020.158056.

[61] Wang Y, Jin J, Zhang M, Wang X, Gong P, Zhang J, Liu J. Effect of the grain size on the corrosion behavior of CoCrFeMnNi HEAs in a 0.5 M H2SO4 solution. J Alloys Compd 2021;858:157712. https://doi.org/10.1016/j.jallcom.2020.157712.

[62] Wang C, Yu Y, Yu J, Zhang Y, Zhao Y, Yuan Q. Microstructure evolution and corrosion behavior of dissimilar 304/430 stainless steel welded joints. J Manuf Process 2020;50:183–91. https://doi.org/10.1016/j.jmapro.2019.12.015.

[63] Senthilkumar S, Manivannan S, Venkatesh R, Karthikeyan M. Influence of heat input on the mechanical characteristics, corrosion and microstructure of ASTM A36 steel welded by GTAW technique. Heliyon 2023;9:e19708. https://doi.org/10.1016/j.heliyon.2023.e19708.